# Downwind Coning Concept Rotor for a 25 MW Offshore Wind Turbine

**Chao (Chris) Qin [*, a], Eric Loth [a], Daniel S. Zalkind [b], Lucy Y. Pao [b], Shulong Yao [c], D. Todd Griffith [c], Michael S. Selig [d], Rick Damiani [e]**

[a] *Department of Mechanical and Aerospace Engineering, University of Virginia*
[b] *Department of Electrical, Computer, and Energy Engineering, University of Colorado Boulder*
[c] *Department of Mechanical Engineering, University of Texas at Dallas*
[d] *Department of Aerospace Engineering, University of Illinois at Urbana-Champaign*
[e] *RRD Engineering*

Manuscript for Renewable Energy

## Abstract

The size of offshore wind turbines over the next decade is expected to continually increase due to reduced balance of station costs per MW and also the higher wind energy at increased altitudes that can lead to higher capacity factors. However, there are challenges that may limit the degree of upscaling which is possible. In this paper, a two-bladed downwind turbine system is upscaled from 13.2 MW to 25 MW, by redesigning aerodynamics, structures, and controls. In particular, three 25 MW rotors have been developed: V1 is the upscaled model, V2 is a partial redesigned model, and V3 is a fully redesigned model. Despite their radically large sizes, it is found that these 25 MW turbine rotors satisfy this limited set of design drivers at the rated condition and that larger blade lengths are possible with cone-wise load-alignment. In addition, flapwise morphing (varying the cone angle with a wind-speed schedule) is investigated in terms of minimizing mean and fluctuating root bending loads using steady inflow proxies for the maximum and damage equivalent load moments. The resulting series of 25 MW rotors, which are the largest ever designed, can be a useful baseline for further development and assessment.

## Keywords:

Offshore wind energy; 25 MW design; downwind turbine model; upscaling

[*] *Corresponding Author*, email: chaoqin@virginia.edu

**NOMENCLATURE**

Roman letters

$A$ = availability

AEP = Annual Energy Production

$C$ = coefficient, scale factor

CA = cone angle

CF = capacity factor

DEL = Damage Equivalent Load

$f$ = distribution function

$k$ = power law factor, Weibull shape factor

$L$ = blade length, wake loss

LCOE = Levelized Cost of Energy

$M$ = mass

MEAN = mean moment

$N$ = parameter to be scaled

$P$ = power

PSD = power spectral density

REBM = root edgewise bending moment

RFBM = root flapwise bending moment

RMS = root-mean-square

s = for a single wind speed

ULT = ultimate load/moment

Greek letters

$\beta$ = cone angle

$\eta$ = scaling factor

$\omega$ = frequency

Subscripts

BM = bending moment

$d$ = drag

$Gen$ = generator

$l$ = lift

max = maximum value

$0$ = original, baseline

$p$ = power

$R$ = rotor

## 1. Introduction

To satisfy the increasing energy demands and protect the planet in an economically attractive manner, renewable and sustainable energy must be further developed. In particular, wind energy is anticipated to become the mainstream energy source throughout the world. The United States Department of Energy (DOE) projects that the fastest growth in U.S. wind energy by 2030 will be led by large offshore turbines, as these systems can capture higher wind speeds aloft and off U.S. coasts, so as to provide utility-scale energy [1]. Increasingly larger and larger wind turbine rotors are anticipated due to generally increased power capture and reduced LCOE (Levelized Cost of Energy). This trend of LCOE improvement is due to generally higher capacity factors and reduced balance of station costs per MW as rotor sizes increase.

Currently, the most powerful wind turbines, either commercially developed or in prototype/demonstration stage, range from 6 to 10 MW. The MHI Vestas V164 is currently the largest production turbine, and it was rated at 8 MW originally and later upgraded to 9.5 MW [2]. For large direct-drive turbines, the 7.58 MW Enercon E-126 is an onshore-only turbine [3], while the Siemens Gamesa SWT-8.0-167-DD is an offshore-only turbine [4]. The largest turbine is Haliade-X from General Electric (GE) that is rated at 12 MW [5]. Most of the largest turbines still have the three-bladed upwind configuration, except the Ming Yang SCD system, which is a two-bladed downwind turbine designed for offshore locations [6].

Meanwhile, several extreme-scale wind turbine models are being generated for research purposes and numerical simulations [7][8][9][10][11]. Many of these use the National Renewable Energy Laboratory (NREL) 5 MW three-bladed upwind turbine [12] as a reference model for the aerodynamic, structural, and control-system properties of a conventional offshore wind turbine. At Sandia National Laboratories (SNL), the NREL 5 MW model was upscaled to 13.2 MW, and a series of 100-meter-length blades were structurally designed and modeled seeking a reduction in blade mass [13]. The SNL-100 rotors were structurally designed by Sandia National Labs based on 100-meter-length blades and the lightest of these is the SNL-100-03 rotor [14]. The UpWind model rated at 5 MW [15] and INNWIND.EU models rated at 10 MW have also been recently upscaled to 20 MW levels [16][17]. The AVATAR model [18] is another 10 MW project in Europe, which has a strong focus on aerodynamics at extreme-scales.

Such wind turbines pose a wide array of technical and economic challenges when combined with a conventional three-bladed upwind turbine design. First, their enormous size leads to very high loads on the blades and the support structures. In particular, once the blade lengths exceed 100 meters (extreme-scales), for an upwind design, the rotor is subjected to much larger thrust-wise and gravity bending loads (relative to the size of centrifugal loads). These increased loads create higher out-of-plane moments that can lead to blade failure and/or tower strike if not properly considered. As a result, the structural design (for ultimate and fatigue loads) becomes quite difficult and generally drives a rotor design to have higher structural mass than might be expected from technology scaling trends [8]. The resulting increased structural mass (and associated cost) of the blades reduces the economic advantages of going towards such extreme-scale turbines.

Thus, limiting blade mass becomes one of the most significant design challenges for extreme-scale turbines. The utilization of advanced high stiffness materials, such as carbon fiber, can help reduce blade mass. However, the blade cost increases significantly with such materials,

and thus cost-effective designs seek to minimize them accordingly for a given blade design. Another key issue with conventional rotors at extreme scales is the size limit in the current blade manufacturing technology, since commercial wind turbine blades are conventionally made in one piece. When the blade lengths exceed 100 meters, this can significantly increase transportation and assembly costs. Another issue associated with conventional rotors at extreme scales is the efficacy of pitch control. Pitch regulation is widely used for large wind turbines, where there is an active controller that can vary the pitch angle of each blade. However, a large and heavy blade has a huge inertia about its pitching axis that will result in a slow pitching speed or increased pitch power requirements. This array of challenges requires new strategies in the design of extreme-scale rotors if they are to drive the next generation of cost-effective wind farms.

One recent approach to address such challenges has been demonstrated at the 13.2 MW level. Using the SNL-100-03 blades as a baseline, a new concept named Segmented Ultralight Morphing Rotor (SUMR) was used to develop a set of 13.2 MW downwind blades [9]. The SUMR-13 blades employed a "pre-aligned" design that has a downwind configuration with a coned rotor, and with the blade number reduced from three to two. Simulation results show that this design can dramatically reduce the mean root flapwise bending moments of the blades, thereby allowing a 25% lower rotor mass while still maintaining the capture area and annual energy production of the SNL-100-03 [14].

In this study, to address the mass and the integral-blade design issues and to respond to the challenges associated with extreme-scale wind turbine systems, the novel two-bladed downwind rotor using downwind load-alignment is further developed and increased in scale to allow an unprecedented 25 MW rated turbine. As shown in Fig. 1, such a turbine dwarfs conventional turbines and is the largest horizontal-axis wind turbine design known to the authors. A set of 25 MW rated rotors are investigated, stemming from an upscaling of the 13.2 MW system in terms of aerodynamics, structural redesign, and controller design. The load-aligned rotor configuration can dramatically reduce the cantilever shear loads and the stiffness requirement on the blades, to allow management of rotor mass, opportunity for straightforward blade segmentation, and even outboard pitching, all aimed towards a reduction in LCOE.

The main objective of the present study is thus to design a 25 MW wind turbine rotor in the context of the key design driving loads with an eventual goal towards a lower LCOE through increased energy capture via a larger rotor. In particular, the focus herein is on increasing annual energy production (AEP) while managing both the mean bending moments and damage equivalent loads (DEL) on the blade roots. The approach in this work starts with upscaling a finalized design

for a 13.2 MW downwind turbine to 25 MW scale for initial evaluation (V1). This is followed by a partially redesigned 25MW design with updated aerodynamics, structures, and control systems (V2). Finally, further improvements are sought in a fully redesigned 25MW rotor that takes into account new design and operating/control features (V3). To the author's knowledge, this is the largest concept design of a wind turbine and the first to show the upscaling for extreme-scale two-bladed downwind turbines. It is also the first to consider active coning (morphing) in terms of detailed flapwise and edgewise loads in combination with annual energy production. The results of the present rotor design study can be used in later studies for a more detailed design that would include tower and generator design aspects as well as a detailed quantification of LCOE.

## 2. Methodology

### 2.1 Upscaling Approach

As noted in the introduction, the SUMR-13 wind turbine models [9] were recently developed using several multidisciplinary codes and solvers to design downwind, two-bladed rotors, to enable ultralight design and low LCOE. The initial 13.2 MW rotor design (SUMR-13A) has a cone angle of 5° and a more advanced version developed (SUMR-13C) has a cone angle of 12.5° with longer blades, where both had a rated wind speed of 11.3 m/s. The tower, drivetrain, and nacelle design were kept the same as the SNL-100-03 models, with blade lengths of 100 meters.

The SUMR-13A and SUMR-13C baseline wind turbine models are herein upscaled to a pair of 25 MW designs (V1 and V2) using analytical scaling rules. The scaling is based on the similarity method with the form of $N = N_0 \cdot \eta^k$, where $N$ is the parameter to be scaled (such as mass, stiffness, and inertia), $\eta$ is the scaling factor, and $k$ is a power law factor that depends on the parameter to be scaled. Herein, the scaling factor is $\eta = L/L_0$, where $L$ is the blade length and $L_0$ indicates the original length of the baseline blade before scaling. The baseline SUMR-13A blade length is 104.35 m, and the first version of the upscaled 25 MW turbine assumes a 150 m blade length. Thus, the scaling factor for the rotor $\eta_R$ is 1.44. This geometric scaling is applied to all external dimensions of the blade. In particular, the chord length of the airfoil in each blade section is scaled by a factor of 1.44, while the airfoil shape and the twist distribution are kept the same. Because the SUMR-13 model employed the SNL100, the scaling factor for the tower, nacelle, and drivetrain is calculated considering the SNL100 blade length, which is 100 m, i.e., the scaling factor for these components is 1.50. Note that scaling can be based on "fixed technology" (no design or topological changes) or based on "advancing technology" (design changes to accommodate increasing scale and new technologies and designs), The former is based on classical beam

mechanics theory while the latter is based on empirical advances that have been demonstrated in the wind turbine industry.

For the fixed technology scaling, the aerodynamic and structural technology are fixed and there is no change in the type nor placement of the materials. Further assuming the moments are primarily based on centrifugal forces and that gravity and thrustwise forces maintain the same relative fraction of influence, the mass scaling would follow the cubic law ($\eta^3$) and the mass moment of inertia follows the quintic law ($\eta^5$). Following this type of scaling, the bending stiffness is the product of the elastic modulus (kept fixed) and the area moment of inertia (which increases by $\eta^4$), so the bending stiffness scaling also follows the quartic law ($\eta^4$). When scaling with the distributed parameters (with "-per-unit-length"), the exponent should be one less than the original. The resulting fixed technology power laws for the nacelle, drivetrain, and tower are shown in Table 1a. The tower height of the 25 MW wind turbine models is about 210 m, while keeping the distributed parameters of the tower with no change. As stated in the objectives, the focus herein is on the rotor and not the nacelle, drivetrain, and tower components, so technology advances were not considered for these components.

For the blade upscaling, however, the power law factors need to be modified to be more realistic. This is especially true for extreme-scale rotors since gravity and thrustwise forces will have increasing influence (relative to centrifugal forces) as rotor size increases. The trend of blade development in practice has shown that the mass scaling power law factor is less than three, due to innovations of the blade design and manufacture. The power factor of 2.1 has been demonstrated for the blade mass upscaling in previous studies [19][20] and is therefore used herein. For the blade stiffness upscaling, the trend is not as clear since it depends on the rotor configuration (upwind or downwind) and the number of blades. For example, an upwind configuration generally requires a stiffer blade than a downwind design in order to avoid blade-tower strikes. In addition, the blade eigenfrequencies need careful considerations to avoid the rotor's rotational forcing. In particular, the two-bladed turbine should prevent (at a minimum) blade resonances at the 2P and 4P frequencies, where $n$P is the $n$-times-per-revolution frequency. Theoretically, a lower mass and/or a stiffer design increases the natural frequency, and vice versa. Based on the above, a power law factor choice of 4.5 was selected for the 25 MW upscaling (instead of 4.0) to provide a safe distance from 2P and 4P for both the flapwise and edgewise frequencies. The scaling factors used for the rotor are listed in Table 1b. This includes scaling for the maximum pitching rate, which affects the capabilities of the control system.

The FAST simulation model was adapted from the SUMR-13 to the upscaled 25 MW model in several steps. First, the tower model (including the distributed mass and stiffness parameters) was scaled from a height of 142 m to 210 m. Next, the blade geometry, mass, and stiffness were upscaled from a length of 104.35 m to 150 m, per Table 1b. The mass-per-unit-length is scaled by $1.44^{1.1}$ and both flapwise and edgewise linear distributed stiffness-per-unit-length parameters are scaled by $1.44^{3.5}$. Then, the generator and the drivetrain parameters of mass and inertia were scaled to 25 MW using the scale factors in Table 1a. Finally, the nacelle dimensions, mass, and inertia were upscaled also using the factors listed in Table 1a. The resulting FAST model was checked to ensure that the tower and blade natural frequencies did not align with any rotor harmonics.

An important parameter to consider in a pitch-regulated wind turbine is the maximum blade pitch rate (in degrees per second). For the NREL 5MW reference turbine, the maximum pitch rate is 8°/s, but rarely exceeds 6°/s during normal operation. Based on the blade's moment of inertia along the pitching axis, the blade torsional moment can be obtained, and it is approximately 200 kN-m at rated wind speeds. To pitch a single blade at 6°/s, the power is about 28 kW (0.56% of 5MW). If we assume the same fraction of power will be used to drive the pitch actuators of a 25 MW system, and also noting that the blade torsion moment has been increased to about 3 MN-m, the maximum pitching speed is reduced to around 2°/s. Thus, the maximum pitch rate scales approximately with $\eta^{-1}$. The maximum pitch rate is a constraint in the Simulink model that includes the controller, FAST turbine model, and pitch actuator. We model the pitch actuator using a low-pass filter. The bandwidth of the 13 MW pitch actuator (0.25 Hz) was scaled to 0.167 Hz for the 25 MW turbine. In this paper, our initial, upscaled model is called "V1".

**2.2 Redesign Approach**

Next, the V1 model is modified and upgraded to the V2 and V3 models with aerodynamic, structural, and control redesign, as shown in Fig. 2. Simulation tools will be discussed in Section 2.3. For the aerodynamic design, both V2 and V3 models continue to use the F1 airfoil family, which was originally designed for the SUMR-13 rotor [23]. The F1 airfoil series is shown in Fig. 3, along with their aerodynamic performance and spanwise distribution. The aerodynamic coefficients ($C_l$ and $C_d$) are calculated within the PROPID code based on the rated condition and the airfoil's radial location. The average Reynolds number is about 20 million, and at the blade tip, the Reynolds number is about 12 million. As noted above, V1 uses the same relative chordwise lengths and twist as that used in the SUMR-13. In contrast, V2 and V3 use different distributions

of chord length and blade twist in order to improve aerodynamic performance based on the power and load requirements at 25 MW.

Note that V1, V2, and V3 all achieve the rated power of 25 MW at the rated wind speed of 11.3 m/s. However, V2 and V3 models employ an axial induction factor of 0.175 to help reduce the loads on the blades for the rated conditions. In order to achieve 25 MW power output at the rated wind speed of 11.3 m/s, the further the rotor is coned, the longer each blade needs to be. For example, the V2 rotor is a scaled-up model based on SUMR-13C and designed with a cone angle of 12.5°, which results in a blade length of 160 m to maintain the rotor capture area so as to meet the power requirement. For the V3 model, the designed cone angle is increased to 22.5°, causing the blade length to further increase to 169 m in order to maintain the capture area. The structural design for the 25 MW V3 model satisfies the tip deflection requirement **Error! Reference source not found.**[32] to avoid tower strike for the extreme loading case. In addition, the design has a safe maximum strain for both flapwise and edgewise loading along the blade span for the extreme loading condition. The fatigue performance was checked by applying normal turbulence wind from cut-in to cut-out wind speeds, demonstrating a fatigue life greater than 20 years for both flapwise and edgewise directions. It is also found that the dynamics and flutter margin for the 25 MW V3 model meets the design requirements with no identified vibration issues and acceptable flutter margin.

For the V3 structural design, the blade mass and stiffness distribution, as well as the material and layouts are redesigned using the blade design tool NuMAD [24] with the corresponding aerodynamics design. The blade mass and stiffness distributions are shown in Fig. 4 for V1-V3, while the 3D view of the final redesigned blade (V3) is presented in Fig. 5. A summary of the three rotor designs is given in Table 2 and the site conditions used for these designs (in line with IEC Class IIB conditions) are listed in Table 3. Shown in Fig. 4, the flapwise stiffness for V1 is large because of the higher spar cap thickness in the 0.1-0.3 span along with a larger chord in this region, compared to the slenderer V2 and V3 designs. With a carbon spar in V2 and V3, this impacts the flapwise stiffness more than the edgewise stiffness. It's also worth noting that the higher edgewise stiffness for both V2 and V3 results from greater trailing edge reinforcement in those designs compared to V1.

After each design iteration, when aerodynamic and structural models are updated, the controller is re-tuned using an automatic tuning algorithm (Fig. 6). The below-rated torque controller is optimized for energy capture. The above-rated pitch controller is based on the NREL-5MW reference controller [12], a gain-scheduled, proportional-integral (PI) scheme. We optimize

the PI gains of the pitch controller to minimize structural loading (and pitch actuation), subject to a constraint on the maximum generator speed during turbulent simulations.

### 2.3 Design Parameters and Simulation Tools

In Table 4, the key design and simulation codes employed in this study are listed. Aerodynamics design is performed using PROPID [21][22][23], which is an inverse rotor design tool that produces a rotor geometry based on desired aerodynamic performance. The desired performance specifications are set by the designer based on power, tip speed ratio, a wind speed distribution, and axial induction along the blade span. Structural design is performed using NuMAD [24]. The structural layup design in NuMAD allows for detailed material stacking and placement along the blade, and the frequency responses of the blades and the tower are calculated by BModes [25].

Aeroelastic simulations are implemented with a series of modules developed by NREL, whereby the core module is FAST (version 8) [26]. Different modules couple wind inflow with aerodynamic and elastic solvers that compute the structural loading on the wind turbine blades and tower. Herein, the turbulent wind inputs are generated by TurbSim [27]. A MATLAB/Simulink interface is developed to process FAST simulations and perform closed-loop control with inputs of generator torque and pitch. Using the FAST results, fatigue is computed using MLife [28][29], which employs a rainflow counting algorithm to determine load cycles and extrapolates them over the lifetime of the wind turbine blades.

## 3. Results and Discussion

### 3.1 Rotors with Fixed Cone Angle and No Teeter

The three rotor designs, each with its own fixed cone angle and all without teeter, are compared in Table 5 based on the same 25 MW rated power. For each of these cases, the inflow was steady with a wind shear profile. The outputs of simulations were in time series, and their mean and root-mean-square (RMS) values were calculated. The mean value provides the average magnitude of the output, while the RMS value describes the range of the output fluctuations. In Table 5, the blade length increases by 12.7% from 150 m (V1) to 169 m (V3), while the blade mass increases by 25.3% from 113.4 Mg to 142.1 Mg. Note that the bending moments and blade deflections are considered at rated conditions only (since this condition leads to the largest operating values).

Due to the large coning angle of 22.5° at rated conditions, the V3 model operates closer to the natural flapwise equilibrium position (dictated by the balance of thrust and centrifugal loads)

than the other models. As such, V3 results in the smallest mean blade root flapwise bending moment (RFBM) even though it has longer and heavier blades. In addition, the higher coning of the V3 rotor yields a large tower-blade clearance to provide increased safety for large blade tip deformation. However, the higher coning angle model has a lower maximum power coefficient ($C_p$). The maximum $C_p$ of the V3 model obtained at rated condition is 0.42, compared to 0.47 for the V2 model. As a reference, when both models are un-coned, i.e. at zero cone angle, they have the same designed maximum $C_p$ value of 0.49. For the fatigue damage analysis on both flapwise and edgewise modes, FAST outputs are used to calculate moment parameters at the rated wind speed: "rated mean" is the time-average, "rated RMS" is the RMS value, and "DEL" is the short-term Damage Equivalent Load (calculated using the MLife code). To compare, the ultimate moment "ULT" is calculated based on the structural design. Exceeding "ULT" will lead to structural failure, and 10% of the ultimate moments (0.1*UTL) are set as the constraints in the present study to ensure consistency with the SUMR-13 design. The flapwise and edgewise results from Table 5 show that a reduction in the mean moments (via load-alignment) for the 25 MW rotor does not generally result in a reduction in the DELs, owing to the increased importance of fluctuating loads at this extreme scale. In particular, the mean edgewise bending moment is relatively small but the fluctuations are large and tend to drive edgewise fatigue. Furthermore, these extreme-scale turbines tend to have DELs that are higher in the edgewise direction than the flapwise direction (which is opposite the general trend for conventional scale turbines). These results are different than that experienced for a two-bladed downwind turbine at 13.2 MW, whereby the flapwise loads dominate and load-alignment allows significant reductions in the DEL values. This indicates that the much larger 25 MW rotor has noticeably different design drivers than a 13 MW rotor. For flapwise loads, the mean moment is greater than the flapwise DEL, and hence requires decreasing the mean moment to satisfy the constraint of 0.1*ULT. However, the mean moment reduction leads to an increase of the RMS moment and the DEL (see V2 and V3 flapwise comparison). It is necessary to determine an approach to restrain the fluctuations, and teeter can help to do so. For edgewise loads, the mean moment is relatively small, and the main contributor to the edgewise DEL is the RMS moment. In the next version of design, it will be considered to replace 18% thickness airfoil to enhance the blade stiffness at the tip while reducing edgewise DEL and saving blade mass. Furthermore, the next section will discuss additional design approaches to reduce both mean and RMS values of flapwise and edgewise bending moments based on the V3 rotor. Moreover, since the flapwise and the edgewise are the defined directions based on the blade itself, pitching the blade can also help to allocate the total loads into two directions. To do so, the pitching operation must to be faster than the variation of the loads.

### 3.2 Rotors with Morphing Schedule

Hinged blades are the norm in helicopter design of two-bladed rotors where strong restoring moments due to centrifugal forces (and gravity) tend to balance aerodynamic bending moments. The equivalent concept for two-bladed rotors on wind turbines is to use teeter, and this can significantly reduce the impact of gravitational and shear loads on the blades [7][8]. Another approach to reduce loads is to employ a variable coning angle, through a morphing schedule as a function of the mean wind speed [31]. The objective of such a morphing schedule is for the rotor to have low coning below the rated condition so as to extract more energy (by opening up the rotor to increase the swept area), and have higher coning above the rated wind speed to reduce mean flapwise bending moments critical to increased loading as well as in extreme conditions. In between, a transition regime is scheduled.

In Fig. 7, the concept of the morphing schedule is shown. The proposed schedule starts at a small cone angle with the rotor at maximum expansion in Region 2 wind speeds so as to maximize energy capture. The coning is actively controlled with actuators operating in a load control mode aiming to maximize energy capture in wind speeds below rated without exceeding a prescribed blade root bending moment limit and tower clearance. As wind speed increases, one approach is to let the rotor cone freely in an average flapwise equilibrium angle (based on downwind aerodynamic and radially outward centrifugal forces) i.e., zero mean flapwise bending moment. The pitch and coning actuators can provide additional flapwise damping to keep the coning angle relatively stable. Since the highest flapwise moments occur at the rated condition, the coning angle can be reduced for wind speeds above rated. However, for such a 25 MW design, the rated flapwise equilibrium position is at a very high cone angle in excess of 45°, so it is impractical to operate at such an equilibrium position. In particular, such a high coning will result in large bending moment increases on the tower and lead to difficulty with yaw control, because the rotor center of mass would move far from the axis of the tower. In addition, a large coning angle will increase the blade root DELs at large wind speed conditions.

Fortunately, V3 shows that a cone angle of 22.5° already provides a large amount of mean flapwise bending moment reduction (Table 5). Therefore, the coning can be limited with a soft-stop to such an angle for these initial morphing designs. In summary, the morphing schedule can be separated into three main portions. In the light wind region (Region 2), shown in the light green color in Fig. 7, the rotor operates at low coning angle to maximize the power output. In Region 2.5, shown in the light blue color, the coning angle is ideally smoothly increased to the maximum operating coning angle as wind speed approaches the rated condition. In Region 3 and beyond,

shown in the light orange color, the coning angle decreases to mitigate the mean bending moments as well as the DELs on the blades. It should be noted that conventional Region 2.5 control (without morphing) is normally limited to a small wind speed range whereby the controller switches from generator torque control to pitch control. This range and strategy of transition is not expected to be modified, such that the morphing control (Region 2.5 morphing) can be considered a slower transition of cone angle super-posed to the faster conventional transition (Region 2.5).

To determine a potential morphing schedule of the 25 MW turbine models, the V3 (fixed coning angle) rotor was used as a baseline to determine a morphing version, V3m, which would allow a variable coning angle. The V3 rotor (length, mass, etc.) was chosen for the baseline since it is a carefully re-designed model that has enough load margin for morphing operations. To explore the potential morphing schedule space, MATLAB was employed to run FAST while varying the wind speed and the coning angle using the V3 blade. The wind speed ranges from 4 m/s (cut-in) to 24 m/s (cut-out) with 1 m/s bins, and at each given wind speed, the coning angle changes from 2.5° to 75° with 2.5° bins. The parameter space yields 630 test conditions to consider. Since this is an impractical number of test cases to run with fully turbulent conditions (especially since this may require adapting the controller for many, if not most, of the cases to ensure consistent performance under optimized control), herein a steady-state inflow approach is considered. A difficult issue with employing steady inflow conditions is that the DEL values for turbulent conditions (usually conventional design drivers) are not known. Therefore, a large safety factor was employed and the constraints are 10% of the ultimate values. This percentage was selected to be consistent with the SUMR-13. While this a conservative approach, it is made more reasonable because of the extreme-scales of the turbines.

To obtain sMEAN, sRMS, and sDEL, where "s" stands for a single wind speed, the FAST code was used to calculate outputs of generator power, blade root flapwise bending moment (RFBM), and blade root edgewise bending moment (REBM) for steady-state inflow conditions for a period of 400 seconds (neglecting the first 50 seconds of numerical transition in simulations). For the whole wind speed range, the simulation outputs are plotted in Fig. 8 by varying the wind speed and the coning angle.

In Fig. 8a, the portion above the rated wind speeds corresponds to a large area of a 25 MW yellow colored plateau in the power output, so no matter how the "path" is chosen in that region, the power output should be the same. Thus, the key to maximizing the power is to determine the "path" when the wind speed is lower than the rated, where moving closer to the horizontal axis is the better choice (higher capture area). In Fig. 8b, the "map" of mean blade tip deflection, is shown,

and although the highly coned rotor has sufficient tower-blade clearance (refer to Table 5), the deflection indicates the degree of load-alignment (i.e., the blade is perfectly aligned when the aeroelastic deflection tends to zero) and the degree of thrust loads (which tends to peak near rated conditions). Interestingly, there are multiple load-aligned angles for wind speeds above 16 m/s. This is due to pitching operations and different pitching strategies. From a practical perspective, the lowest load-aligned coning angle will reduce the complexity of the morphing mechanism and avoid the practical issues noted above for high coning angles.

The "map" of sMEAN for the flapwise bending moment (Fig. 8c) is qualitatively similar to Fig. 8b, where the peak is located near the rated wind speed and smallest cone angle. Avoiding this region but choosing a smaller coning angle away from the rated conditions will tend to provide the largest power output below rated and the lowest tower bending moments above rated. The sDEL of the flapwise bending moment is shown in Fig. 8d, where there is an increase as wind speed and coning angle increase. To minimize the fatigue damage, the "path" should be close to the horizontal axis to minimize sDEL, especially when the wind speed is large. However, Fig. 8e and Fig. 8f indicate that the morphing schedule based on the edgewise bending moments can be equally, if not more, problematic than the flapwise bending moments. It is important to note that gravitational loading, which occurs almost purely in the edgewise direction for small cone angles, is present to a larger extent in the flapwise direction as cone angle increases. Therefore, a morphing schedule that reduces the flapwise bending moments will effectively reduce the impact of gravitational loadings, which has beneficial consequences for structural design.

Based on the above contours, a morphing schedule to effectively maximize the power output while limiting the four moment-based design drivers (sMEAN and sDEL for flapwise and sRMS and sDEL for edgewise) can be created by making a coning angle selection for each wind speed. In particular, the above contour maps in their discrete state as a function of wind speed and cone angle can be interrogated to provide a total number of $30^{21}$ different morphing schedules of cone angle as a function of wind speed. To narrow down the possible schedules, the maximum coning angle is limited to 22.5°, and in Region 3, the coning angles are required to decrease as wind speed increases so as to minimize flapwise DELs. This reduces the total number of possible morphing schedules to about 20,000. The number of schedules can be further reduced by eliminating any schedule which produces a flapwise sMEAN, edgewise sRMS or both flapwise and edgewise sDEL that is greater than the maximum allowable value for V3 flapwise moments (155.3 MN-m), or for V3 edgewise moments (152.7 MN-m). The most critical of the four moment-

based design drivers investigated was found to be flapwise sMEAN, followed by edgewise sDEL, flapwise sDEL, and edgewise sRMS.

To consider the annual energy production (AEP) output of the wind turbine for a fixed rated power (the generator is held fixed for all these simulations), the capacity factor can be defined as

$$\mathrm{CF} = \left( \sum_{v_{\text{cut-in}}}^{v_{\text{cut-out}}} f_{weibull}\left(v_i\right) P_{Gen,i} \right) \cdot A \cdot \left(1 - L\right) / P_{rated}$$

where $f_{weibull}$ is the Weibull distribution function of a given wind speed and $P_{Gen}$ is the rated generator power output. The summation of their product is multiplied by an average availability of 92.2% ($A$), and an estimated wake loss of (1-$L$), where $L$ is 9.96%. Then the capacity factor results for a given morphing schedule is normalized by the CF of V3 ($\mathrm{CF}/\mathrm{CF}_0$), where $\mathrm{CF}_0$ is 0.44 for the fixed coned baseline rotor. Note this capacity factor ratio is equivalent to ($\mathrm{AEP}/\mathrm{AEP}_0$) such that a high value can help minimize LCOE.

In Fig. 9a, all possible "paths" within these constraints are shown in terms of the normalized capacity factor and the most sensitive design driving load normalized by its maximum allowable value (0.1*ULT). In Fig. 9a, each blue circle represents a potential morphing schedule, and each schedule has a calculated AEP and flapwise sMEAN, both of which are normalized by their values at a fixed constant coning angle of 22.5°. Meanwhile, the open red squares stand for different fixed coned rotors where cone angles decrease going from left to right and V3 is the solid red square. It can be seen that decreasing cone angles can increase the power output but the trade-off is the flapwise sMEAN increases as well. The constraint value for flapwise sMEAN is about 155 MN-m. Compared with the fixed coned rotors, most of the morphing cases perform better in terms of generating more energy. The selected morphing schedule indicated by the green triangle has the longest distance among all the candidates to the trade-off line, and the schedule is shown in Fig. 9b and Fig. 9c. The trade-off line is determined by a ratio of 10, i.e. 10% loads increase for 1% energy increase. The selected schedule has all the characteristics mentioned previously with increased AEP and limited flapwise sMEAN by the constraint. In this schedule, the rotor is opened up to a constant coning angle of 7.5° at low wind speed to capture more energy from the wind, and then the rotor is coned to the designed 22.5° around the rated wind speed. When the wind speed goes above the rated, the coning angle decreases and becomes aligned with the zero-mean RFBM line shown in Fig. 9b. In Fig. 9c, the morphing schedule shows that operating conditions remain within the edgewise constraint, which is about 150 MN-m. Since the spacing of the coning angle is 2.5° in the simulation, to obtain a smooth morphing schedule, a smaller spacing is suggested.

The morphing schedule balances between the load reduction and the energy increases. For example, the morphing schedule at the wind speed of 10 m/s shown in Figs. 9b and 9c could have a larger cone angle to further reduce both the RFBM sMEAN as well as REBM sDEL values. However, a larger cone angle will sacrifice more energy capture. Thus, in the morphing schedule, the cone angle for 10 m/s is chosen to yield the best tradeoff between loads and power output, as determined from Fig. 9a.

The morphing effects can be quantified in AEP and lifetime DEL calculations listed in Table 6. The V3 model with fixed cone angle has an AEP of 3853 MW-hr/MW. As a comparison, the AEP values of the V2 model with fixed angle and the 13.2 MW conventional baseline design are 3580 and 3385 MW-hr/MW respectively. The results also show that the primary driver for DEL for the 25 MW rotors is the large fluctuating contribution from the variable thrust and gravity loads. This is different from the case of conventional-scale turbines, where turbulent fluctuations are often the primary driver for DEL. This allows a first–order estimate of the values that might be seen in turbulent conditions. Both are based on the full range of steady flow conditions from cut-in to cut-out. Additionally, note that lifetime DEL can be understood as the average sDEL weighted by wind speed distribution. Thus, the lifetime value is usually less than the maximum value found at a single wind speed shown previously in Fig. 9. Compared with the fixed coned rotor case, morphing can provide an AEP increase of 6%, and the maximum of the flapwise sMEAN increases 21% (still under the constraint of 155.3 MN-m) as trade-off. Morphing has less effect on the edgewise lifetime DEL, but it can help to reduce the maximum edgewise sMEAN by 43%, which mainly results from pitching. It is also worth noting that 25 MW turbines can produce more energy per unit of power than 13.2 MW conventional turbines, demonstrating the trend of large wind turbine development. In summary, the aim to limit loads via a larger coned rotor to the levels of the baseline design was successful, and the morphing provides one solution for the extreme-scale rotor to reduce the flapwise loads while maintaining an increase in AEP. However, it should be noted that this rotor concept design is incomplete as it does not consider a full suite of IEC standard load conditions (yaw, parked cases, power failure, etc.). Furthermore, there will be significant impacts on the tower and drivetrain for these different rotors that are not considered.

### 3.3 Future Options for Load Reduction

As shown above, the edgewise loads are not significantly mitigated by morphing for loads. This becomes a significant challenge as the rotor size increases and the edgewise moments become more design driving than the flapwise moments and other loads. Recalling the edgewise moments listed in Table 5, the edgewise fluctuations have a large contribution to the fatigue damage.

Significantly pitching a rotor can transfer edgewise loads to flapwise loads by geometrically moving the blade chord out of the rotational plane, especially for a coned rotor. Thus, edgewise fluctuations (which drive rotor mass and cost) may be partially mitigated by integrating a fast-response pitching system that has enough bandwidth to cover the frequency spectrum of the fluctuations. As noted by the scaling, the maximum pitching speed is reduced to around 2°/s for a 25 MW turbine. This can be seen in terms of the power spectral density (PSD) of REBM shown in Fig. 10 as a function of normalized frequency (normalized by the maximum pitch speed). Energy content above a normalized frequency of units is thus beyond the bandwidth capability of the pitch control. For the NREL 5 MW case, about 98% of the PSD is distributed within the pitch control region, so this is not a significant concern. But for the upscaled 25 MW system, the largest energy peak is located outside of the pitch control region, and 65% of PSD is above the pitch response frequency. One option to address this issue is an outboard pitching concept illustrated in Fig. 11. Because the mechanism only rotates the outer part/segment of the blade, which is lighter, this control system has faster articulation. Blade segmentation is facilitated by the reduced shear loads at projected joint locations (via morphing) and will substantially reduce fabrication and transportation costs. The outboard articulation of segments #2 and #3 is facilitated by the segmentation and the fact that the outer portions have high aerodynamic authority combined with low mass and inertia. This articulation eliminates all inboard pitch to provide faster and more distributed aerodynamic control (as compared to pitching the entire blade) which increases control authority and system robustness, key differentiators from conventional wind turbines. Further study on the outboard articulation and segmented blade concepts is recommended to determine the impact on capacity factor, loads and structural mass, as well as ultimately the impact on LCOE.

**5. Conclusions**

A series of three 25 MW rotor designs have been examined at a range of wind speeds with steady and turbulent conditions in terms of maximum and damage equivalent blade moments, tower-blade clearance and frequency response to pitch control. This paper had three main objectives. The first objective was to upscale a 13.2 MW wind turbine system to a 25 MW design with a downwind two-bladed configuration. This was accomplished using scaling laws to develop the V1 model. The second objective was to upgrade the V1 model's aerodynamics and structural design as well as controller tuning. The V2 and V3 models were successfully developed and simulated with FAST and other codes, and they satisfied the design requirements to operate at high coning angles. Thirdly, the V3 model was employed to show the capability of integrating morphing to increase the wind energy capture while limiting the loads. As a result, the series of 25 MW rotors, which are the largest ever designed, can be a useful baseline for further development and

assessment. This paper also discussed a technical feasibility idea to further reduce the edgewise loads when using outboard pitching with the present 25 MW wind turbine models. In addition, the extreme-scale of these wind turbine rotors indicate that blade segmentation may be key technology at this scale. Future work includes further improving the V3 design to reduce edgewise loads, validating with IEC standards, and enabling outboard articulation in the simulation codes.

**Acknowledgements**

This work was supported and funded in part by the Advanced Research Projects Agency – Energy (ARPA-E), U.S. Department of Energy, under Award Number DE-AR0000667. The fourth author also gratefully acknowledges support from a Palmer Endowed Chair Professorship.

**References**

[1] *Wind Vision: A New Era for Wind Power in the United States* (U.S. Department of Energy, 2015)

[2] de Vries, E., 2017. *MHI Vestas Launches 9.5 MW V164 Turbine in London.* (https://www.windpowermonthly.com/article/1435504/mhi-vestas-launches-95mw-v164-turbine-london)

[3] Goudarzi, N. and Zhu, W.D., 2013. A review on the development of wind turbine generators across the world. *International Journal of Dynamics and Control*, *1*(2), pp. 192-202.

[4] Arrambide, I., Zubia, I. and Madariaga, A., 2019. Critical review of offshore wind turbine energy production and site potential assessment. *Electric Power Systems Research*, *167*, pp. 39-47.

[5] Winters, J. and Saunders, Z., 2018. The Largest Wind Turbine Ever. *Mechanical Engineering Magazine Select Articles*, *140*(12), pp. 31-31.

[6] Koh, J.H. and Ng, E.Y.K., 2016. Downwind offshore wind turbines: Opportunities, trends and technical challenges. *Renewable and Sustainable Energy Reviews*, *54*, pp. 797-808.

[7] Loth, E., Steele, A., Qin, C., Ichter, B., Selig, M.S. and Moriarty, P., 2017. Downwind pre-aligned rotors for extreme-scale wind turbines. *Wind Energy*, *20*(7), pp. 1241-1259.

[8] Noyes, C., Qin, C. and Loth, E., 2018. Pre-aligned downwind rotor for a 13.2 MW wind turbine. *Renewable energy*, *116*, pp. 749-754.

[9] Zalkind, D.S., Ananda, G.K., Chetan, M., Martin, D.P., Bay, C., Johnson, K.E., Loth, E., Griffith, D.T., Selig, M.S. and Pao, L.Y., 2019. System-Level Design Studies for Large Rotors. *Wind Energy Science*, Vol. 4, pp. 595-618, https://doi.org/10.5194/wes-4-595-2019

[10] Ashuri, T., Martins, J.R., Zaaijer, M.B., van Kuik, G.A. and van Bussel, G.J., 2016. Aeroservoelastic design definition of a 20 MW common research wind turbine model. *Wind Energy*, *19*(11), pp. 2071-2087.

[11] Ashuri, T., Zaaijer, M.B., Martins, J.R. and Zhang, J., 2016. Multidisciplinary design optimization of large wind turbines—Technical, economic, and design challenges. *Energy conversion and management*, *123*, pp. 56-70.

[12] Jonkman, J., Butterfield, S., Musial, W. and Scott, G., 2009. *Definition of a 5-MW reference wind turbine for offshore system development*. National Renewable Energy Laboratory, NREL/TP-500-38060, Golden, CO.

[13] Griffith, D.T. and Ashwill, T.D., 2011. *The Sandia 100-meter all-glass baseline wind turbine blade: SNL100-00*. Sandia National Laboratories, SAND2011-3779, Albuquerque, NM.

[14] Griffith, D.T. and Richards, P.W., 2014. *The SNL100-03 blade: Design studies with flatback airfoils for the Sandia 100-meter blade*. Sandia National Laboratories, SAND2014-18129, Albuquerque, NM.

[15] Barlas, T.K. and van Kuik, G.A.M., 2009. Aeroelastic modelling and comparison of advanced active flap control concepts for load reduction on the upwind 5MW wind turbine. *Proc. European Wind Energy Conference and Exhibition*.

[16] Jensen, P.H. and Natarajan, A., 2014. INNWIND. EU. Overview of project and recent results. In *EERA DeepWind 2014-11th Deep Sea Offshore Wind R&D Conference*.

[17] Sartori, L., Bellini, F., Croce, A. and Bottasso, C.L., 2018. Preliminary design and optimization of a 20MW reference wind turbine. In *Journal of Physics: Conference Series* (Vol. 1037, No. 4, p. 042003). IOP Publishing.

[18] Schepers, J.G., Boorsma, K., Sørensen, N., Sieros, G., Rahimi, H., Heisselmann, H., Jost, E., Lutz, T., Maeder, T., Gonzalez, A. and Ferreira, C., 2018. Final results from the EU project AVATAR: Aerodynamic modelling of 10 MW wind turbines. *Journal of Physics: Conference Series* (Vol. 1037, No. 2, p. 022013). IOP Publishing.

[19] Jamieson, P. and Hassan, G., 2011. *Innovation in wind turbine design* (Vol. 2, No. 2.4). Chichester: Wiley.

[20] Kairuz Fonseca, S., 2017. Estimation of the Optimum Wind Turbine Size for Two Different Offshore Sites and Wind Farm Rated Powers.

[21] Selig, M.S. and Tangler, J.L., 1995. Development and application of a multipoint inverse design method for horizontal axis wind turbines. *Wind Engineering*, pp. 91-105.

[22] Selig, M. S., PROPID – Software for Horizontal-Axis Wind Turbine Design and Analysis, http://www.ae.illinois.edu/m-selig/propid.html.

[23] Ananda, G.K., Bansal, S. and Selig, M.S., 2018, Aerodynamic Design of a 13.2 MW Segmented Ultralight Morphing Rotor. *AIAA SciTech Forum,* AIAA Paper 2018-0994, Kissimmee, FL, January 2018.

[24] Berg, J.C. and Resor, B.R., 2012. *Numerical manufacturing and design tool (NuMAD V2. 0) for wind turbine blades: User's guide.* Sandia National Laboratories, SAND2012-728, Albuquerque, NM.

[25] Bir, G., 2005. *User's Guide to BModes (Software for Computing Rotating Beam-Coupled Modes)*. National Renewable Energy Laboratory, NREL/TP-500-39133, Golden, CO.

[26] Jonkman, J.M. and Buhl Jr, M.L., 2005. *FAST user's guide.* National Renewable Energy Laboratory, NREL/EL-500-38230, Golden, CO.

[27] Jonkman, B.J. and Buhl Jr, M.L., 2006. *TurbSim user's guide.* National Renewable Energy Laboratory, NREL/TP-500-39797, Golden, CO.

[28] Hayman, G., 2012. *MLife theory manual for version 1.00*. National Renewable Energy Laboratory, Golden, CO.

[29] Hayman, G.J. and Buhl Jr, M., 2012. *MLife user's guide for version 1.00*. National Renewable Energy Laboratory, Golden, CO.

[30] Moriarty, P.J. and Hansen, A.C., 2005. *AeroDyn theory manual*. National Renewable Energy Laboratory, NREL/TP-500-36881, Golden, CO.

[31] Ichter, B., Steele, A., Loth, E., Moriarty, P. and Selig, M., 2016. A morphing downwind-aligned rotor concept based on a 13-MW wind turbine. *Wind Energy*, *19*(4), pp. 625-637.
[32] Yao, S., Griffith, D.T., Chetan, M., Bay, C.J., Damiani, R., Kaminski, M. and Loth, E., 2019. Structural Design of a 1/5th Scale Gravo-Aeroelastically Scaled Wind Turbine Demonstrator Blade for Field Testing. *AIAA Scitech Forum*, AIAA Paper 2019-1067, San Diego, CA, January 2019.

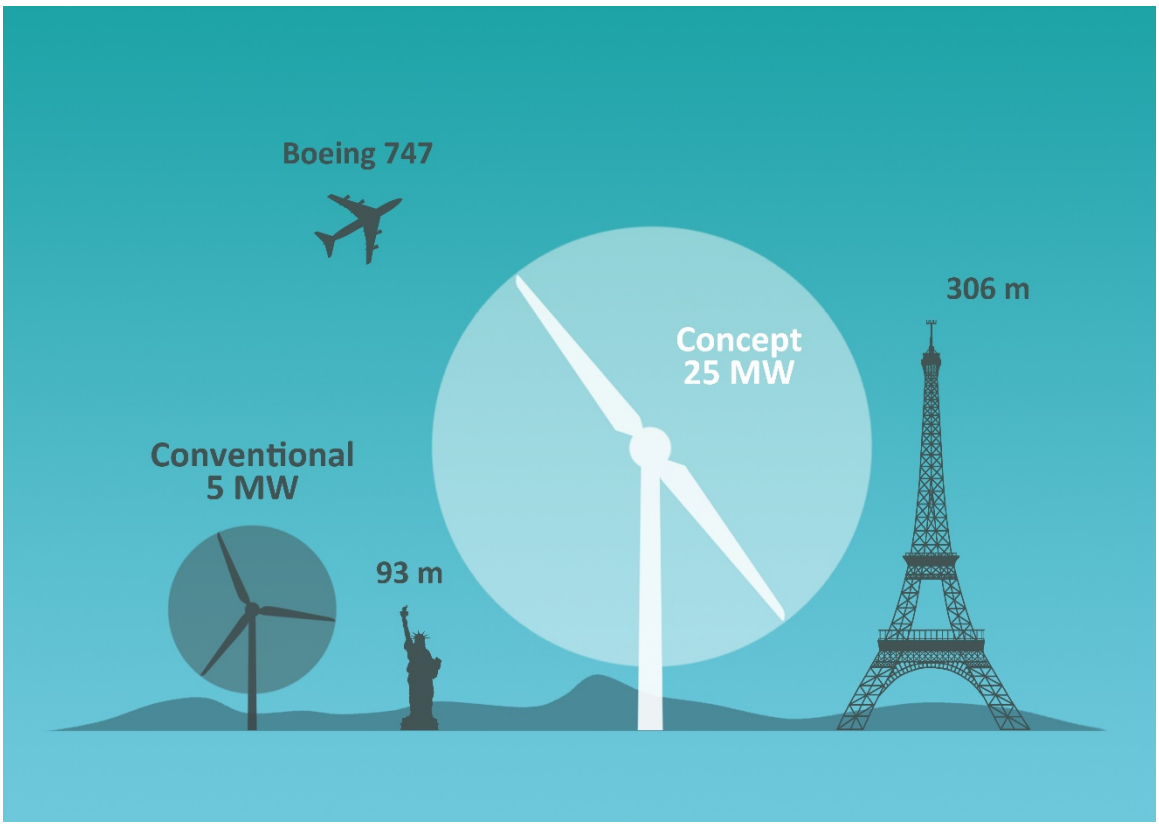


Fig. 1 Graphic view of the 25 MW two-bladed downwind turbine and comparison of its size with the conventional 5 MW three-bladed upwind turbine

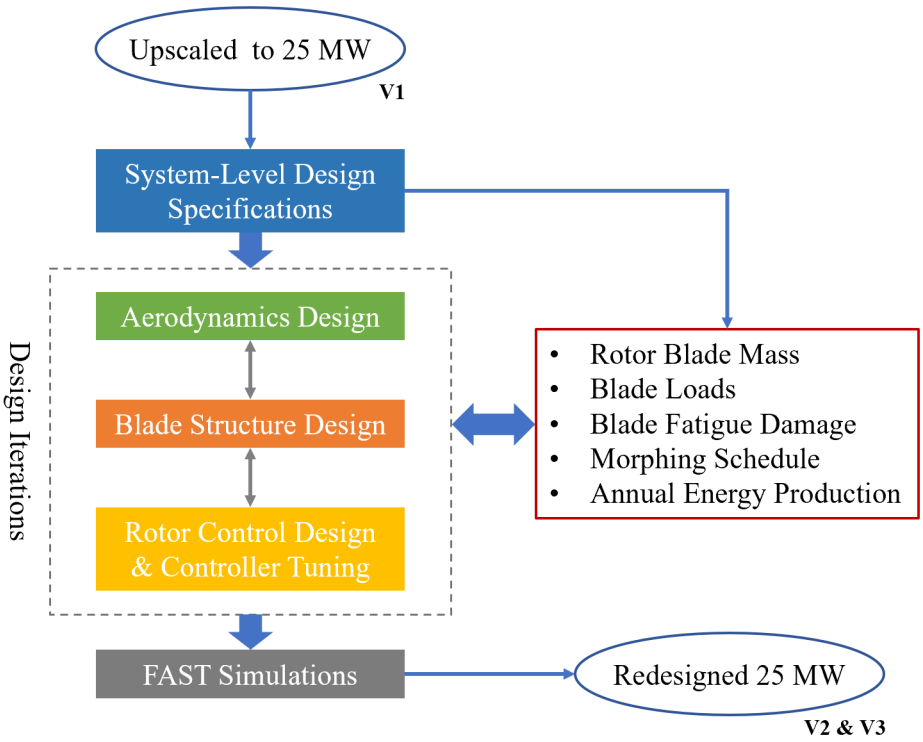


Fig. 2 Rotor re-design process and design iterations among aerodynamics, structure, and control

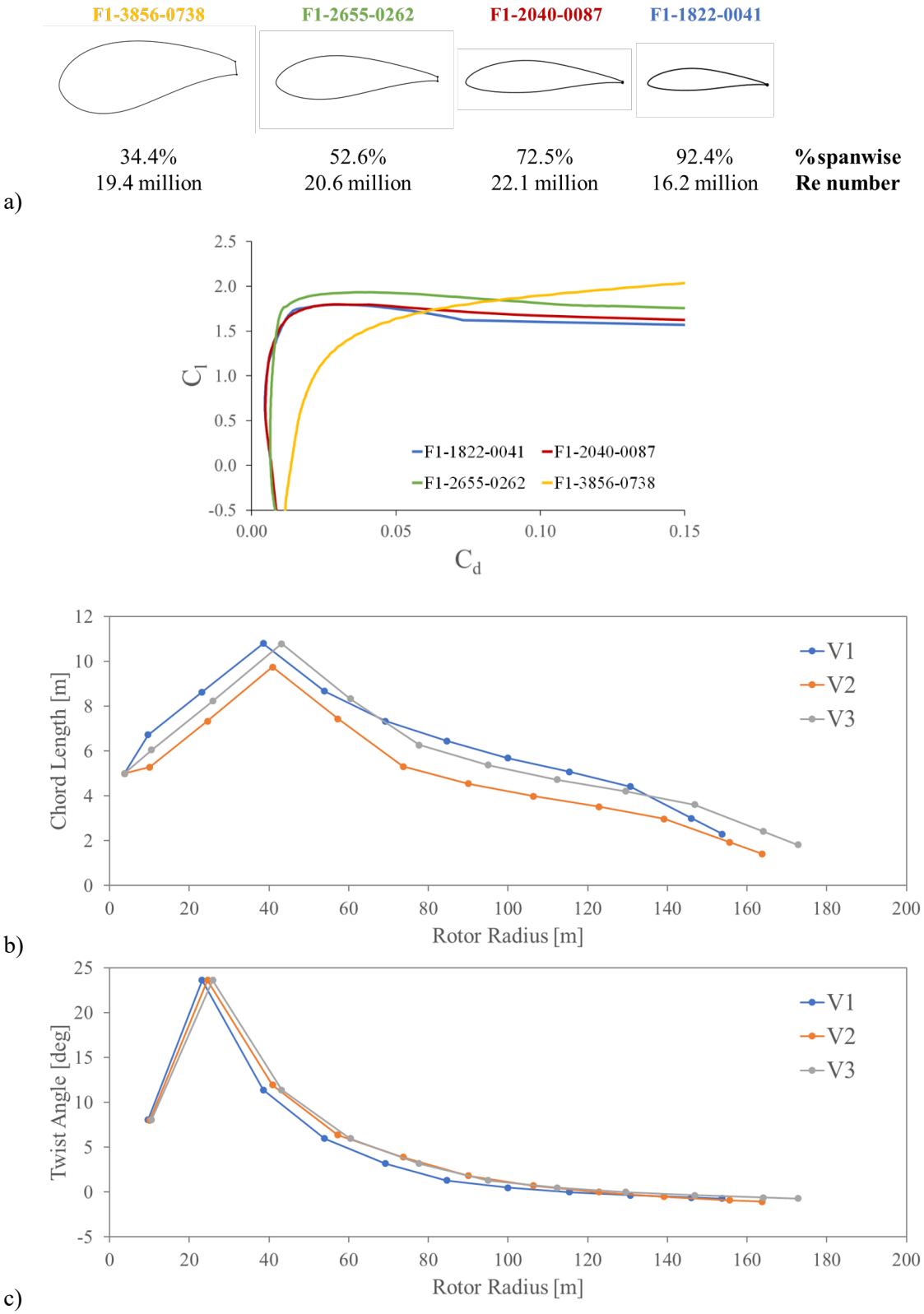


Fig. 3 a) the F1 Series airfoils and their $C_l$ vs. $C_d$ curves, b) chord length schedule, and c) twist angle distribution for the V1, V2, and V3 25 MW blade designs

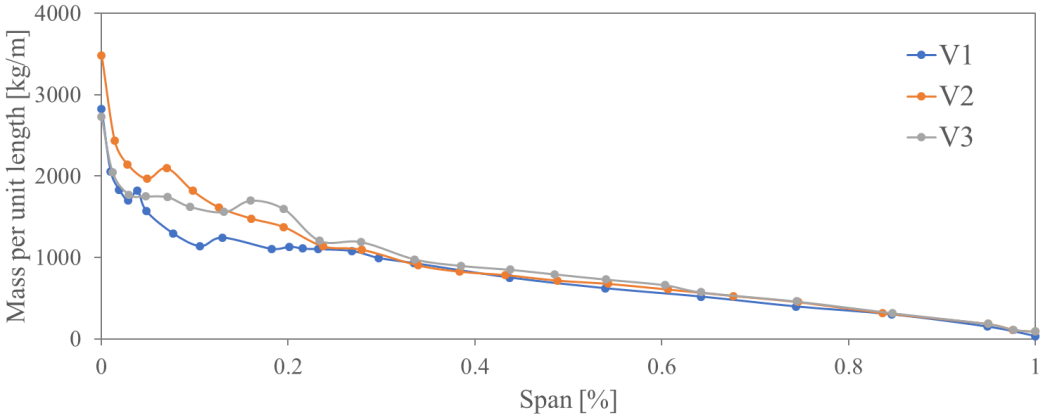


a)

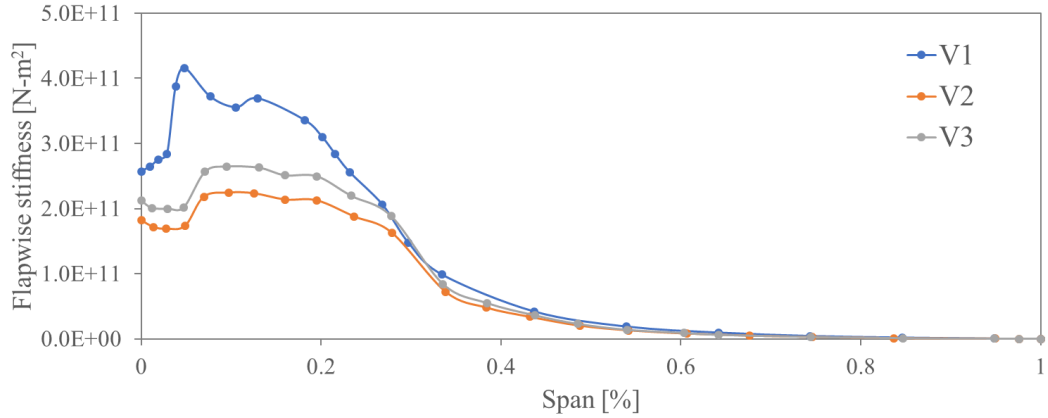


b)

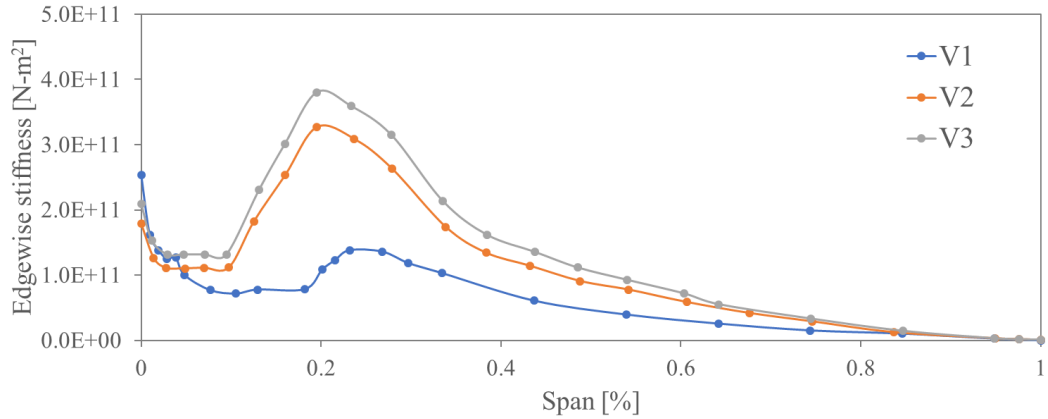


c)

Fig. 4 Blade spanwise distributions of mass and stiffness (flapwise & edgewise) for the three different 25 MW rotor designs

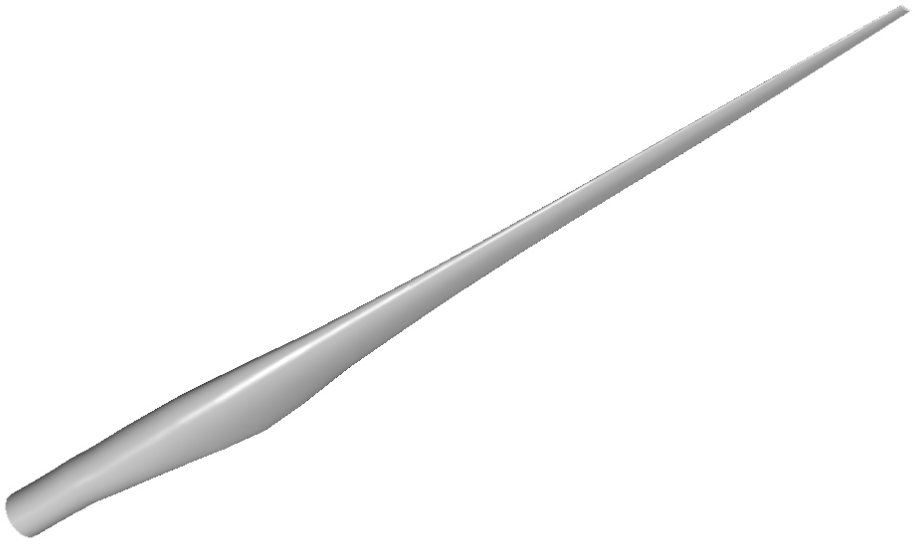

Fig. 5 3-D view of the redesigned 25 MW wind turbine V3 blade

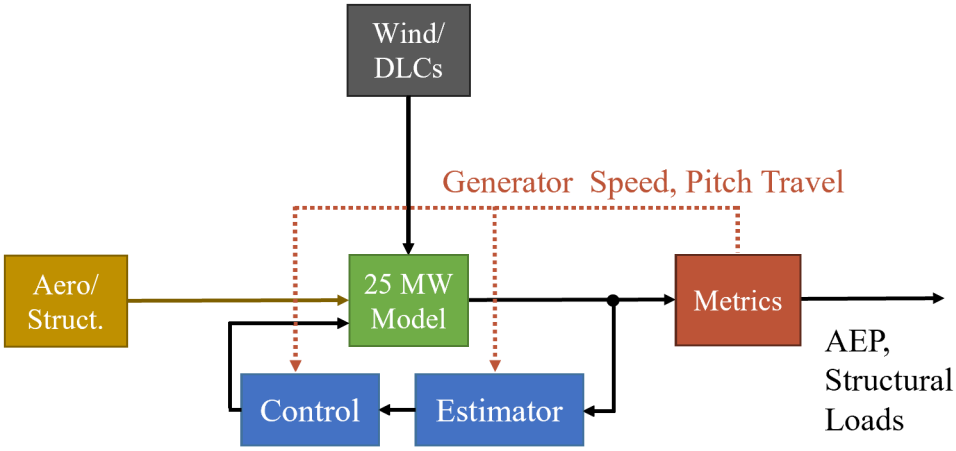


Fig. 6 Aerodynamics, structural, and control designs are iterated to achieve a 25 MW wind turbine design that yields acceptable AEP, structural loads, generator speed regulation, and pitch travel.

Table 1a Power laws used for upscaling to the 25 MW turbine components ($\eta$ = 1.50)

| Component | Parameter | Power Law | Notes |
|---|---|---|---|
| Drivetrain | Mass | $\eta^3$ | Fixed technology scaling |
| | Inertia | $\eta^5$ | Fixed technology scaling |
| | Power | - | Scaled to 25 MW |
| Nacelle | Dimension | $\eta^1$ | Geometric scaling |
| | Mass | $\eta^3$ | Fixed technology scaling |
| | Inertia | $\eta^5$ | Fixed technology scaling |
| Tower | Dimension | $\eta^1$ | Height adjusted to 210 m |
| | Mass | $\eta^3$ | Fixed technology scaling |
| | Stiffness | $\eta^4$ | Fixed technology scaling |

Table 1b Power laws used for upscaling to the 25 MW turbine blade/rotor ($\eta$ = 1.44)

| Component | Parameter | Power Law | Notes |
|---|---|---|---|
| Blade/Rotor | Dimension | $\eta^1$ | Geometric scaling |
| | Mass | $\eta^{2.1}$ | Advanced technology scaling |
| | Linear mass density | $\eta^{1.1}$ | Advanced technology scaling |
| | Stiffness (flapwise and edgewise) | $\eta^{4.5}$ | Using Campbell resonance diagram and simulations |
| | Linear stiffness (flapwise and edgewise) | $\eta^{3.5}$ | Using Campbell resonance diagram and simulations |
| | Maximum pitching rate | $\eta^{-1.2}$ | Advanced technology scaling with fixed % of power consumption |

Table 2 Main design parameters for the three different 25 MW turbine models

| Parameter | Description | Units | Design Version | | |
|---|---|---|---|---|---|
| | | | V1 | V2 | V3 |
| $\beta$ | Design cone angle | deg | 5.0 | 12.5 | 22.5 |
| $R_{\text{rotor}}$ | Rotor radius | m | 153.75 | 163.75 | 172.75 |
| $R_{\text{hub}}$ | Hub radius | m | 3.75 | 3.75 | 3.75 |
| $L_{\text{blade}}$ | Blade length | m | 150 | 160 | 169 |
| $M_{\text{blade}}$ | Blade mass | Mg | 113.4 | 134.6 | 142.1 |

Table 3 Environmental and aerodynamics design parameters for the 25 MW turbine models

| **Parameter** | **Value** |
|---|---|
| Wind class | Class II |
| Turbulent intensity | Level B |
| Shear exponent | 0.1 |
| Rated electrical power | 25 MW |
| Hub height | 210 m |
| Rated wind speed | 11.3 m/s |
| Cut-in wind speed | 4 m/s |
| Cut-out wind speed | 24 m/s |
| Mean wind speed | 9.08 m/s |
| Weibull shape, scale factor | $k = 2.167$, $C = 10.25$ |
| Air density | 1.21 kg/m$^3$ |
| Kinematic viscosity | $1.48 \times 10^{-5}$ m$^2$/s |
| Maximum power coefficient ($C_{p,max}$) | 0.493 |
| Tip speed ratio at $C_{p,max}$ | 9.45 |
| Fine pitch angle | 0.476° |

Table 4 Computational codes used for the 25 MW model design and simulation processes

| Tool / Software | Function |
|---|---|
| PROPID [22] | Inverse aerodynamic design code for blade geometry |
| NuMAD [24] | Create 3D models of blade materials and structures |
| TurbSim [28] | Generate turbulent wind field inputs |
| AeroDyn [30] | Simulate unsteady aerodynamic forces |
| FAST v8 [26] | Simulate the aeroelastic dynamic response of wind turbines |
| BModes [25] | Calculate modal frequencies of blades |
| MLife [29] | Estimate the fatigue damage on blades |
| Simulink | Implement the advanced controller |
| MATLAB | Implement the whole simulation processing |

Table 5 Rotor design comparisons (no teeter) based on steady rated conditions (11.3 m/s)

| Model | | V1 | V2 | V3 |
|---|---|---|---|---|
| Blade | Length [m] | 150 | 160 | 169 |
| | Mass [Mg] | 113.4 | 134.6 | 142.1 |
| Cone Angle | [deg] | 5.0 | 12.5 | 22.5 |
| Rotor | Diameter [m] | 306.3 | 319.7 | 319.2 |
| Root **Flapwise** Bending Moment [MN-m] | sMEAN | 173.2 | 90.1 | 82.6 |
| | sRMS | 18.5 | 18.3 | 29.2 |
| | sDEL | 48.9 | 43.9 | 69.1 |
| | ULT | 1589 | 1761 | 1553 |
| Root **Edgewise** Bending Moment [MN-m] | sMEAN | 14.2 | 14.2 | 18.2 |
| | sRMS | 41.5 | 50.7 | 57.8 |
| | sDEL | 95.6 | 126.3 | 131.8 |
| | ULT | 1567 | 1740 | 1527 |
| Tip Deflection [m] | rated mean | 13.3 | 11.2 | 12.9 |
| | rated RMS | 1.34 | 1.78 | 2.64 |
| Clearance [m] | Undeflected | 8.2 | 30.1 | 60.3 |
| | Minimum | 19.6 | 38.8 | 69.5 |

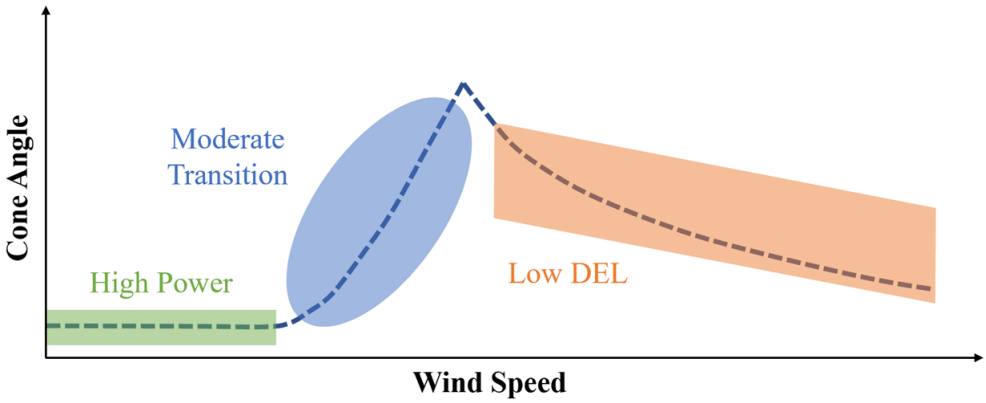


Fig. 7 Sketch of a morphing schedule for operation of a 25 MW coning rotor

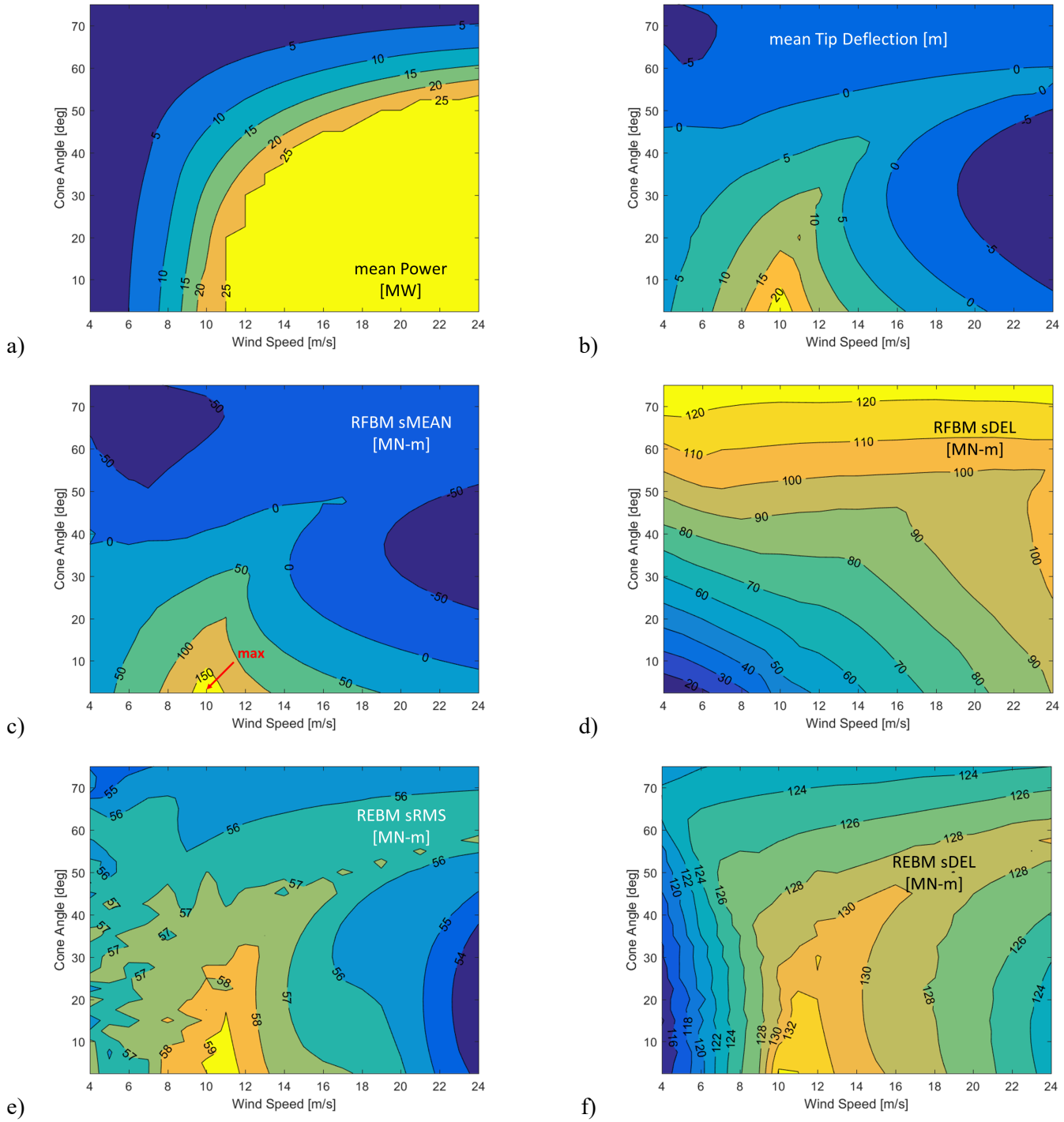


Fig. 8 FAST steady inflow simulation contours of the V3 model with varying wind speeds and coning angles: a) mean generator power output, b) mean blade tip deflection, c) flapwise sMEAN, d) flapwise sDEL, e) edgewise sRMS, and f) edgewise sDEL.

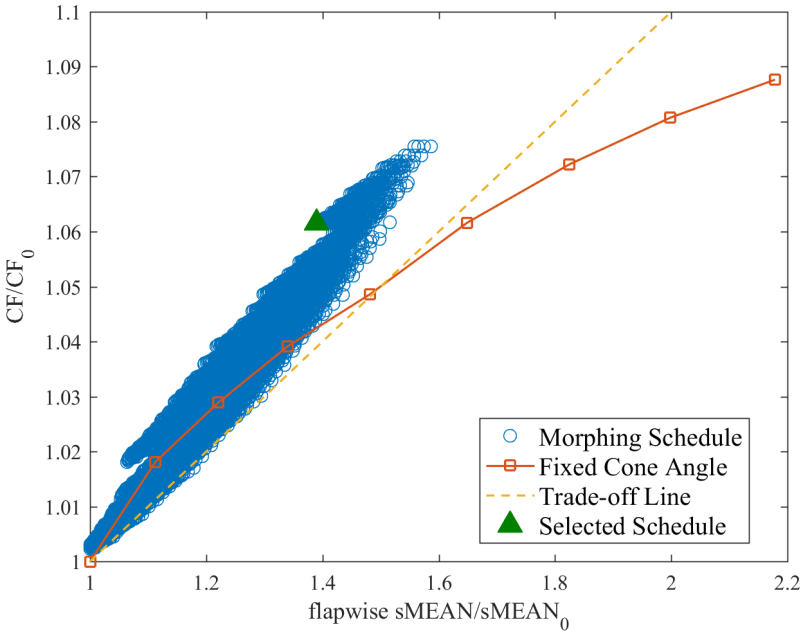


a)

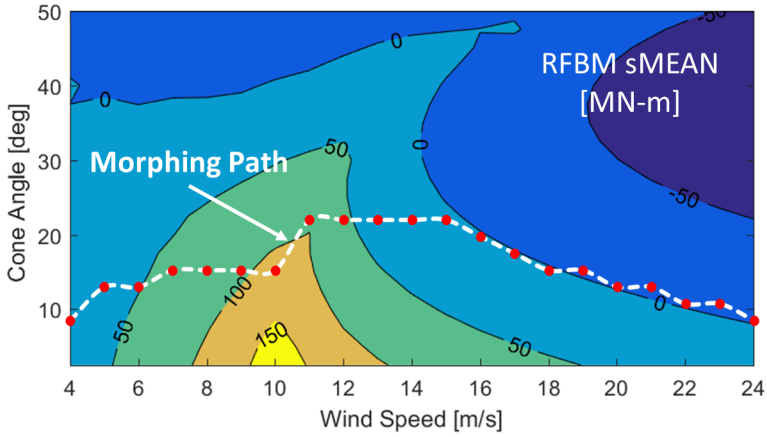


b)

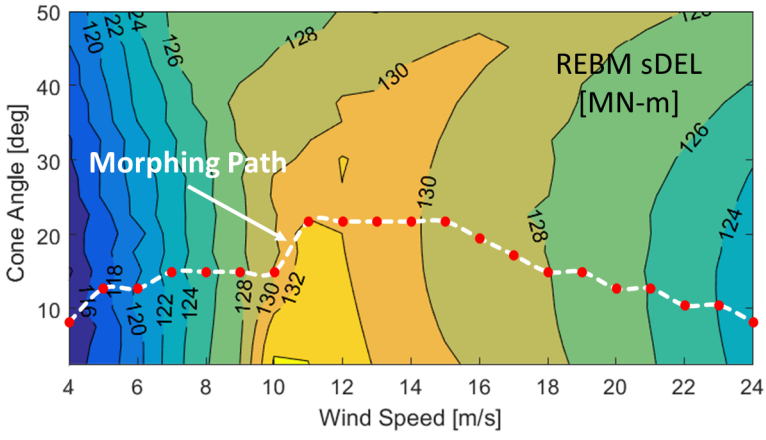


c)

Fig. 9 Morphing schedules a) trade-off between CF and flapwise sMEAN, b) & c) selected path

Table 6 Comparisons between fixed coned and morphing rotors for full range of flow conditions

| | **13.2 MW Conventional** | **25 MW V3 Fixed CA** | **25 MW V3 Morphing** |
|---|---|---|---|
| AEP [MW-hr/MW] | 3,385 | 3,853 (0%) | 4,090 (+6.2%) |
| **Flapwise max sMEAN [MN-m]** | **-** | **94.4 (0%)** | **114.1 (+20.9%)** |
| Flapwise rated sMEAN [MN-m] with turbulent inflow+ | - | 71.6 | 71.6 |
| Flapwise max sRMS [MN-m] | - | 42.3 (0%) | 40.3 (-4.7%) |
| Flapwise rated sRMS [MN-m] with turbulent inflow+ | - | 50.2 | 50.2 |
| Flapwise Lifetime DEL [MN-m] | - | 58.1 (0%) | 49.4 (-15.0%) |
| Edgewise max sMEAN [MN-m] | - | 41.3 (0%) | 23.7 (-42.6%) |
| Edgewise rated sMEAN [MN-m] with turbulent inflow+ | - | 21.0 | 21.0 |
| Edgewise max sRMS [MN-m] | - | 58.3 (0%) | 58.3 (0%) |
| Edgewise rated sRMS [MN-m] with turbulent inflow+ | - | 58.7 | 58.7 |
| **Edgewise Lifetime DEL [MN-m]** | **-** | **114.0 (0%)** | **114.0 (0%)** |

* **bold** indicates design driving loads

+ both 25 MW cases have same CA = 22.5° at rated turbulent inflow

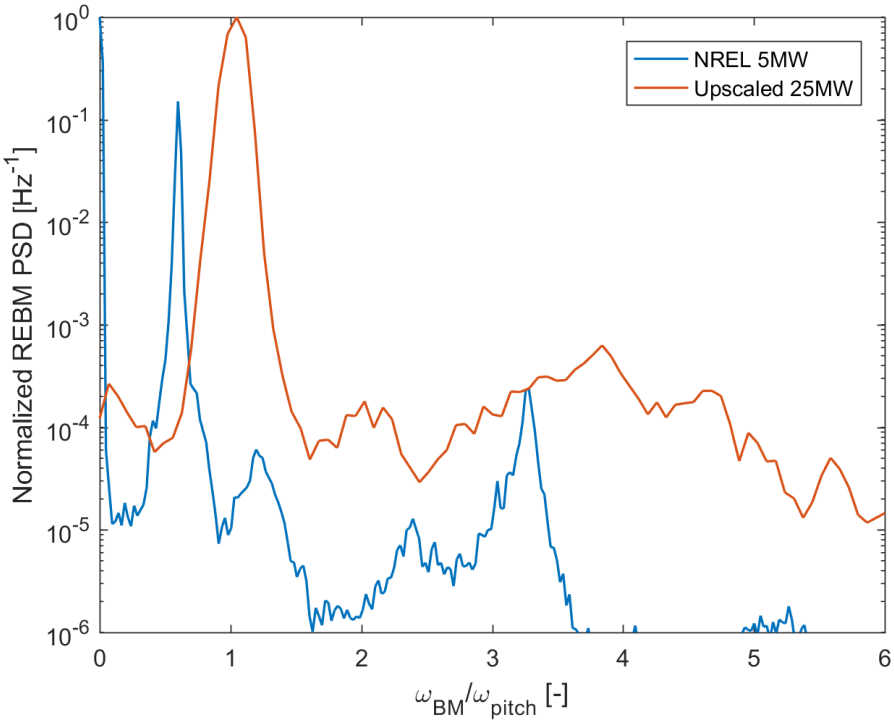


Fig. 10 Normalized power spectral density of REBM at rated turbulent wind condition, and the frequency is normalized by the maximum pitch speed

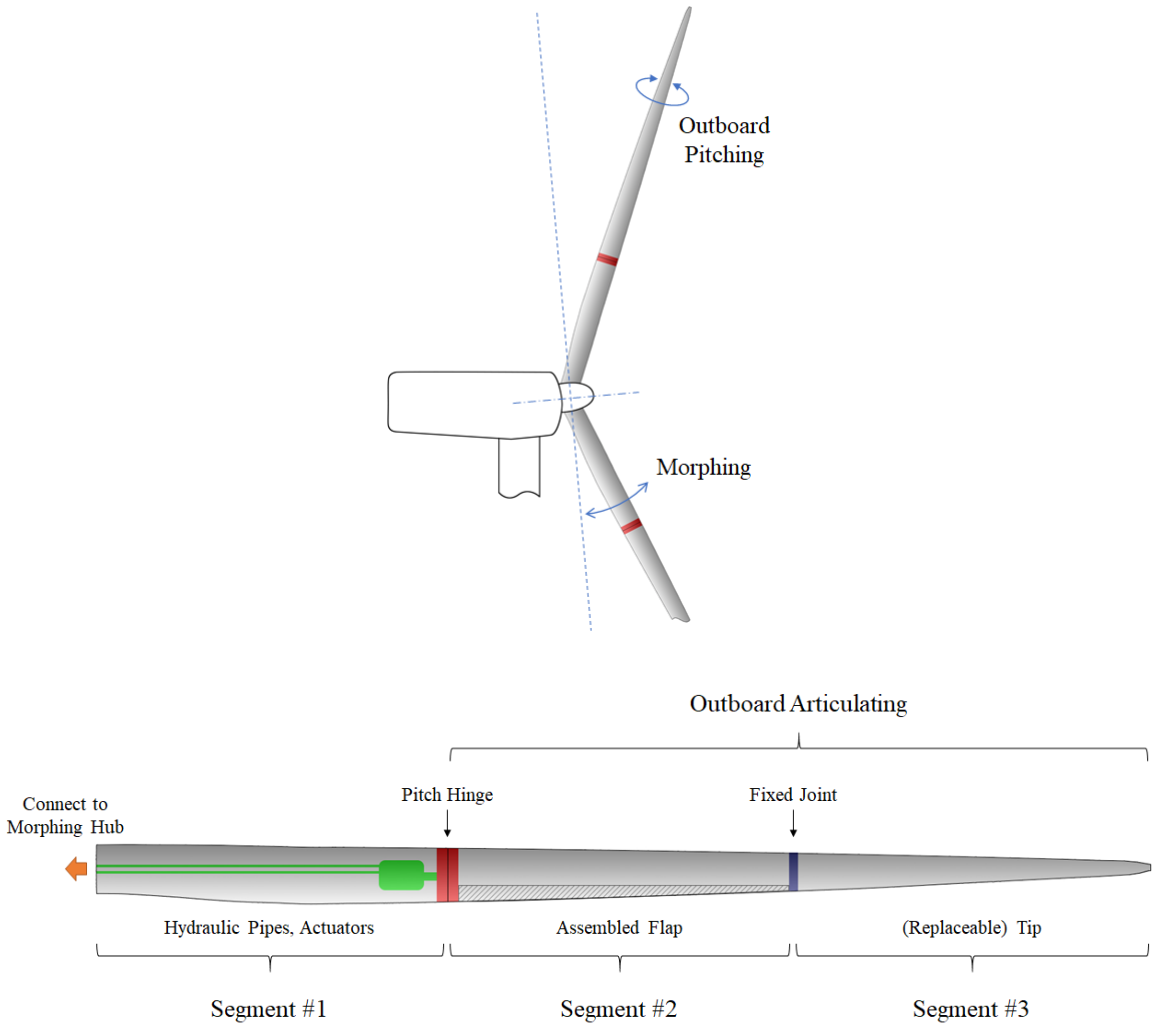


Fig. 11 Sketch of blade segmentation, outboard pitching, and morphing